HIGH PERFORMANCE MSG SATELLITE MODEL FOR OPERATIONAL SOLAR ENERGY APPLICATIONS

Tomáš Cebecauer
GeoModel, s.r.o.
Pionierska 15
841 07 Bratislava, Slovakia
tomas.cebecauer@geomodel.eu

Marcel Šúri
GeoModel, s.r.o.
Pionierska 15
841 07 Bratislava, Slovakia
marcel.suri@geomodel.eu

Richard Perez
State University of New York
Atmospheric Sciences Research Center,
251 Fuller Rd
Albany, NY, 12203
perez@asrc.cestm.albany.edu

ABSTRACT

We present a new version of model for high-performance calculation of global and direct irradiances from Meteosat Second Generation (MSG) satellite data covering Europe, Africa and Middle East. The full spatial and temporal resolutions of MSG data are used. The model philosophy is based on the principles of Heliosat-2 calculation scheme and the model by [1]. The advancements of the model enabled to enhance spatial resolution and to decrease Bias and RMSE in hilly terrain, high mountains, coastal and arid zones, and for periods with snow coverage.

1. INTRODUCTION

A number of satellite-based solar radiation models have been developed using Heliosat scheme, e.g. [1], [2], [3], [4], to mention a few. In general, accuracy of satellite-derived solar radiation models suffers in mountains, complex coastal zones, at low sun angle, and in period with snow. Since 2004 Meteosat MSG satellite offers data at high resolution: every 15 minutes, 12 spectral channels, at a grid resolution of approx. 1 km and 3 km in sub-satellite point. The information potential of MSG data is still not fully exploited, although substantial improvements in methodology were made [5], [6].

The operational use and delivery of gridded data in near-real time on a continental scale still poses challenges due to large volume of data, complexity of algorithms and geographical variability. In Europe a significant part of population lives in mountains where terrain affects exploitation of solar energy.

In this article we present innovative features of MSG-based satellite model for more accurate and fast calculations.

2. MSG MODEL IMPROVEMENTS

Model enhancements include: (1) multi-spectral satellite information to improve classification of snow/land/cloud signals, (2) a new algorithm to find lower bound (LB) values preserving diurnal variability, (3) implementation of backscatter correction (4) variable upper bound for dynamic range and cloud index calculations, (5) simplified SOLIS clear sky model, and (6) downscaling with high resolution DEM to include local variability of solar irradiance.

2.1 MSG multi-spectral data processing

Four MSG spectral channels were used in a classification scheme to distinguish clouds from *snow* and *no-snow cloud-free* situations. Prior to the classification, calibrated pixel values were transformed to three indexes: (i) normalized difference snow index [7], (ii) cloud index [8], and (iii) temporal variability index. Reflectance values of VIS006 and IR_016 channels, and brightness temperatures of IR_039, IR_108 channels along with spectral and variability indexes and sun geometry were used in a decision tree classifier to assign pixels to classes.

The cascade of pixel classification tests proposed by [5] for the Alpine region was modified to deal with spectral

response of geographically distinct regions within our area of interest, which extends from North Europe to North Africa. The satellite data calibration coefficients maintain the radiometric stability of the grid cell values and they allow using the same fixed thresholds in the classification decision tree for both Meteosat-8 (MSG1) and Meteosat-9 (MSG2) data. As a result, for each pixel the class id (snow, snow-free land or water, cloud and unclassified) was assigned for each time slot.

The classification results are afterwards enhanced by post-classification filtering, to clean isolated classes within a day and check subsequent-day coherence. The filtering improved classification, mainly in situations with broken clouds and cloud shadows.

Exploiting the potential of MSG spectral data for snow classification removed the need of additional ancillary snow data and allowed using spectral cloud index information in cases of complex conditions such as clouds over high albedo snow areas.

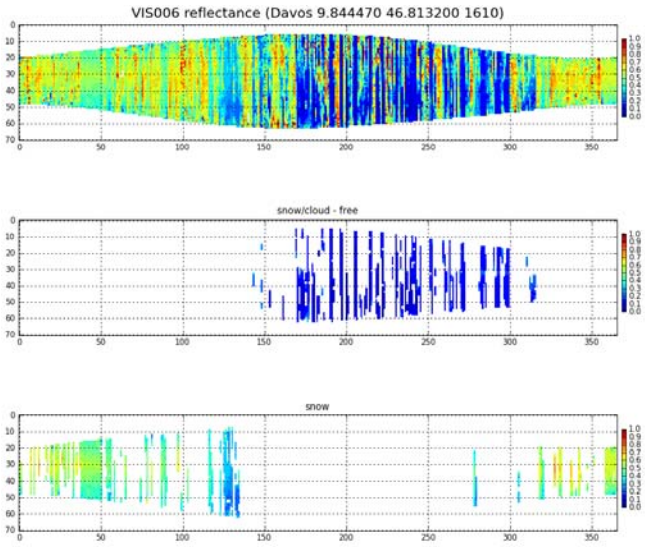

Fig. 1: Example of the classification output for Davos, Switzerland. From top: a) reflectance for VIS006 channel, b) classification for cloud-free land, c) cloud-free snow, clouds. X-axis represents day-of-year, Y-axis time slot of satellite image (bottom morning, top evening).

2.2 Calculation of surface pseudo-albedo

In the original approach by [1], the identification of surface pseudo-albedo is based on the use of a lower bound (LB), representing cloudless situations. It is derived as an average value of low reflectance pixels within moving time window that results in one LB value per day. This approach neglects diurnal variability of LB that is later corrected by statistical approach. To overcome this limitation other models, e.g. [9] analyze the pseudo-albedo individually for each time slot. However, limiting the lowest value search to one slot increases probability that in a given time window no cloudless situation exists.

To overcome these problems, the identification of LB in the new model is based on a use of all classified cloudless values in a moving time window. Instead of identifying one value per day, LB is represented by smooth 2-dimensional surface (in day and time slot dimensions) that reflects diurnal and seasonal changes in LB and reduces probability of no cloudless situation. The LB surface is approximated by quantile regression [10] with variable weights over the moving time window.

To allow representation of the LB by smooth surface the local increase of reflectivity in low sun-ground-satellite angles was removed by backscatter correction [11]. Similarly to the original approach by [1], the length of moving time window is reduced in a case of snow presence.

2.3 Cloud index

Overcast conditions represented in the original Perez model by a fixed Upper Bound (UB) value were updated to account for spatial variability which is important especially in the higher latitudes. Calculation of cloud index was extended by incorporation of snow classification results. For very high LB values, cloud index is calculated from spectral cloud index. Although sensitivity of spectral cloud index to cloud optical thickness is lower, but in extreme cases may perform better than standard CI scheme or specifying artificial lower and upper bounds as proposed by [5].

2.4 Clear sky model SOLIS and solar components

Broadband simplified version of SOLIS model [12] was implemented. On the input of this model, we used climatology values from the NVAP water vapor database [13] and Atmospheric Optical Depth data by [14] assimilated with AERONET [15] and AEROCOM datasets.

Simplified Solis model was implemented into DIRINDEX algorithms to calculate Direct Normal Irradiance component

[16]. Diffuse irradiance for inclined surfaces is calculated by updated Perez model [17].

2.5 Downscaling solar irradiance with high resolution terrain information

Processing chain of the new model includes post-processing terrain disaggregation algorithm that is based on the approach by [18]. The authors showed that corrections of the satellite estimates in a complex terrain resulted in a reduction of the mean bias up to 13% for cloudless days with low sun altitude, and over 2% for cloudy conditions and high sun altitude.

The disaggregation in our approach is limited to shadowing effect only, as it represents most significant local effect of terrain. The algorithm uses local terrain horizon information with spatial resolution of 100 m. Direct and circumsolar diffuse components of global irradiance were corrected for terrain shadowing. The adopted approach showed strong influence of terrain on irradiance pattern in complex terrain environment.

3. MODEL PERFORMANCE

Results are compared with high-quality ground measurements from 50 stations over Europe and North Africa (Fig. 2), 5 stations being located in high altitudes.

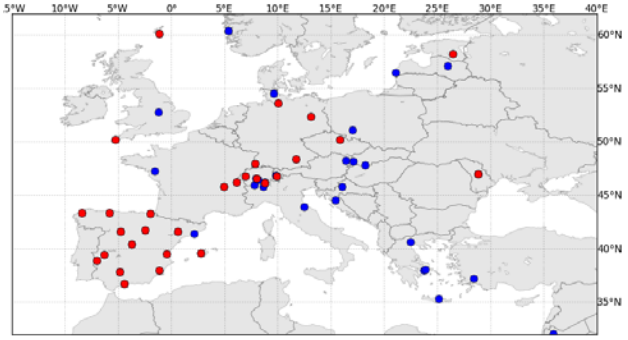

Fig. 2: Sites used for the model validation. Data available: blue – Global Horizontal Irradiance, red – Direct Normal and Global Horizontal Irradiance.

The overall relative mean bias difference (rMBD) for Global Horizontal Irradiance (GHI) is -1.4%, and relative root mean square difference (rRMSD) is 20.0%, 10.7% and 4.7% for hourly, daily and monthly data, respectively. For 30 stations the rMBD of Direct Normal Irradiance (DNI) is -2.5%, and rRMSD is 38.2%, 24.4% and 10.7%, respectively.

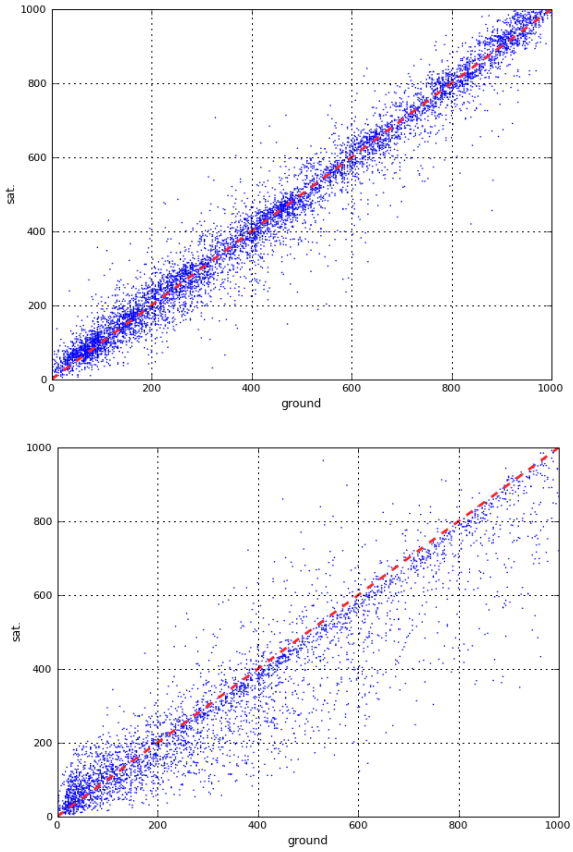

Fig. 3: Comparison of modelled Global Horizontal Irradiance with high-quality ground measurements. Top: arid region (Badajos, Spain), bottom: Davos (mountainous region, Switzerland). Slight underestimation of the clear-sky irradiance in Davos results from the overestimation of Atmospheric Optical Depth in a complex terrain of high mountains.

The model improvements are seen especially in the mountains, coastal zones, and arid areas. Compared to previous results (project MESoR, 2007-2009 [19]), the GHI overall bias of the new model in the high mountains of the Alps is between -8% and +4% and rRMSD around 30%, which shows significant improvement by the presented approach.

The new lower bound approach with diurnal variability shows substantial improvements in arid zones – for GHI hourly values in central Spain the rRMSD is around 14%,

for sites in deserts (Tamanrasset and SedeBoqer) the rRMSD goes below 12%.
Implementation of backscatter correction has negligible effect on the summary statistics of the model, but improves representation of diurnal profiles of irradiation (Fig. 4).

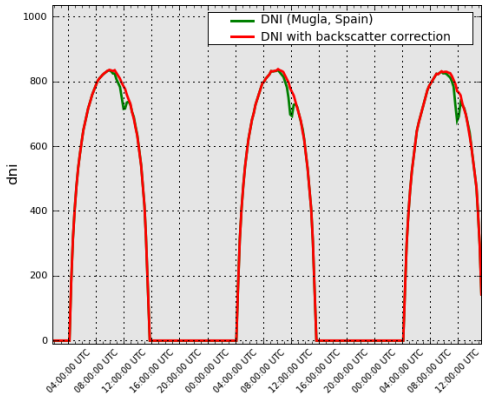

Fig. 4: Daily profiles of direct normal irradiance from model without backscatter correction (green) and with correction (red) for Mugla, Spain October 2-4, 2006.

4. DATA AVAILABILITY

The new model is routinely used to calculate solar radiation for Europe, North Africa and the Middle East covering the MSG period (from 2004 up to present) at full data resolution of SEVIRI instrument. The adoption of simplified version of SOLIS model makes the new algorithmic chain prepared to read more atmospheric data at higher time and spatial resolution once they are available.

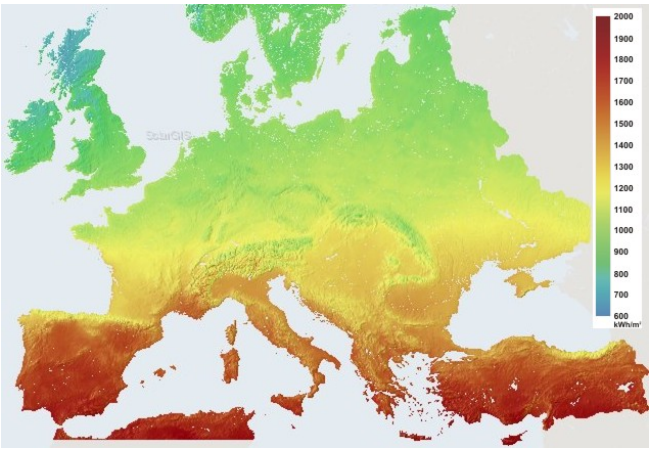

Fig. 5: Global Horizontal Irradiation – long-term average for the period 2004-2009 in kWh/m^2

The distributed computing and efficient data storage make it possible to derive and process data for any site or region in real-time.

The primary database of GHI, DNI and derived parameters (Fig. 5) at high resolution and different time-aggregation domains covers the most recent years from 2004 to 2010. It is available from http://solargis.info.

5. ACKNOWLEDGMENTS

This work was co-funded by the Slovak Research and Development Agency under the contract No. VMSP-P-0042-07. We thank to Pierre Ineichen for consultations and critical comments.

6. REFERENCES

1. R. Perez, P. Ineichen, K. Moore, M. Kmiecik, C. Chain, R. George, F. Vignola, A New. Operational Satellite-to-Irradiance Model, *Solar Energy*, 73, 2002, 307-317.
2. Hammer A., Heinemann D., Hoyer C., Kuhlemann R., Lorenz E., Müller R., Beyer H.G., 2003. Solar energy assessment using remote sensing technologies. *Remote Sensing of Environment*, 86, 423–432.
3. Müller, R.W., Dagestad, K., F., Ineichen, P., Schroedter-Homscheidt, M., Cros, S., Dumortier, D., Kuhlemann, R., Olseth, J.A., Piernavieja, G., Reise, C., Wald, L., Heinemann, D. 2004. Rethinking satellite-based solar irradiance modelling. The SOLIS clear-sky module. *Remote Sensing of Environment*, 91, 160-174.
4. Rigollier, C., Lefèvre, M., Wald, L., 2004. The method Heliosat-2 for deriving shortwave solar radiation from satellite images. *Solar Energy* 77, 159-169.
5. B. Dürr; A. Zelenka, Deriving surface global irradiance over the Alpine region from METEOSAT Second Generation data by supplementing the HELIOSAT method, *International Journal of Remote Sensing*, 2009, 30, 22, 5821-5841
6. LandSAF 2006 – Down-welling Surface Short-Wave Radiation Flux. Product Manual. SAF/LAND/MF/ PUM_DSSF/1.4
7. M. Ruyter de Wildt, G. Seiz, A. Gruen, 2007. Operational snow mapping using multitemporal Meteosat SEVIRI imagery, *Remote Sensing of Environment*, 109, 29-41.

8. M. Derrien, H. Gleau, MSG/SEVIRI cloud mask and type from SAFNWC, *International Journal of Remote Sensing*, 26, 4707-4732.
9. Verdebout, J., 2000. A method to generate surface UV radiation maps over Europe using GOME, Meteosat, and ancillary geophysical data, *Journal of Geophysical Resources*, 105(D4), 5049–5058.
10. R. Koenker, K.F. Hallock, Quantile Regression. *Journal of Economic Perspectives*, 2201,15 143-156.
11. R. Kuhlemann, A. Hammer. Sunsat the new program for processing high resolution data of Meteosat-8. 2005, *Heliosat-3 project*.
12. P. Ineichen, A broadband simplified version of the Solis clear sky model, Solar Energy, 2008, 82, 8, 758-762.
13. D. Randel, T. H Vonder Haar, M.A. Ringerrud, G. L. Stephens, T.J. Greenwald C.L. Combs, A New Global Water Vapour Dataset. *Bulletin of the American Meteorological Society*. 1996, 77, 1233-1246.
14. J. Remund, Updated Linke Turbidity and aerosol optical depth climatologies, 2008, *IEA SHC Task 36 expert meeting*, June 2008, Wels, Austria.
15. AERONET (AErosol RObotic NETwork) program, http://aeronet.gsfc.nasa.gov/
16. R. Perez, P. Ineichen, E. Maxwell, R. Seals, A. Zelenka, Dynamic global to direct irradiance conversion models. *ASHARE Trans. Res. Series*, 1992, 354-369
17. R. Perez, R. Seals, P. Ineichen, R. Stewart, D. Menicucci, A New Simplified Version of the Perez Diffuse Irradiance Model for Tilted Surfaces. Description Performance Validation. *Solar Energy*, 1987. 39, 221-232.
18. J.A. Ruiz-Arias, T. Cebecauer, J. Tovar-Pescador, M. Šúri, 2010. Spatial disaggregation of satellite-derived irradiance using a high resolution digital elevation model, accepted to *Solar Energy*.
19. C. Hoyer-Klick et al., MESoR – Management and Exploitation of Solar Resource Knowledge, *Conference SolarPACES 2009*, Berlin.